Numerical Investigation of Polymer Craze Growth and Fracture

F. Xiao

Hewlett-Packard Company, San Diego, California 92127

W. A. Curtin*

Department of Engineering Science and Mechanics and Department of Materials Science and Engineering, Virginia Polytechnic Institute and State University, Blacksburg, Virginia 24061-0219

Received June 29, 1994; Revised Manuscript Received November 8, 1994®

ABSTRACT: The craze formation and failure typical of many glassy polymers have been investigated using an elastic spring network to model both bulk and crazed polymer material. The elastic properties of the network springs were modified, using simple rules, to capture the bulk polymer to crazed material deformation and the subsequent failure of the craze. The resulting self-consistent evolution of the craze zone and craze failure due to a stress concentration in the craze material at the original crack tip are in basic agreement with experimental observations and with other theoretical predictions of the general features of crazing polymers.

I. Introduction

For many amorphous polymers, especially brittle or glassy polymers, the failure of the material is related to the stress-induced growth and breakdown of crazes. In the present work, we introduce a simple tractable model to self-consistently simulate the initiation, propagation, and breakdown of the craze in a bulk polymer using simple physical rules extracted from experimental results. The model, to be discussed below, captures the essential qualitative features of the crazing process and supports recent mechanics models of the craze breakdown phenomenon.

Crazes are planar, cracklike defects (see Figure 1a) usually formed ahead of a crack tip. A schematic microscopic craze structure is given in Figure 1b. When the applied tensile stress or strain reaches a critical value, voids are nucleated, and the polymer is drawn out of the bulk phase from an "active" zone, which is a thin boundary layer between the bulk polymer phase and the crazed phase, to form craze fibrils, which range in diameter from 5 to 30 nm.[1] These fibrils bridge the two bulk polymer surfaces and have load-bearing ability, thereby shielding the crack tip from the applied stress intensity. The main fibrils align themselves with the maximum tensile stress direction, which is the crack-opening direction in mode I crack problems.[2] Stress concentration at the craze tip drives the craze forward while further drawing of the fibrils from the bulk material widens the craze zone. The drawing process occurs at the natural draw ratio of the polymer, which is almost a constant at a given drawing speed and temperature, and so the fibril volume fraction remains unchanged in the craze zone as the craze widens.[1−4]

Recent studies have shown that short "cross-tie" fibrils connect the main aligned fibrils in the craze (Figure 1b). Such cross-ties are formed from polymer strands too strong to be separated when the main fibrils are drawn out of the bulk phase, such that it is more favorable for the whole strand to be pulled out to form a cross-tie fibril than to break the cross-tie.[5] These cross-tie fibrils give the craze weak load-bearing ability in the direction perpendicular to the crack-opening direction.[1] The cross-ties allow stress to be transferred from one main fibril to another main fibril, which generates stress concentrations and ultimately contributes to fibril breakage. The role of cross-ties in establishing a stress concentration in the main fibrils is a primary concern in the present work.

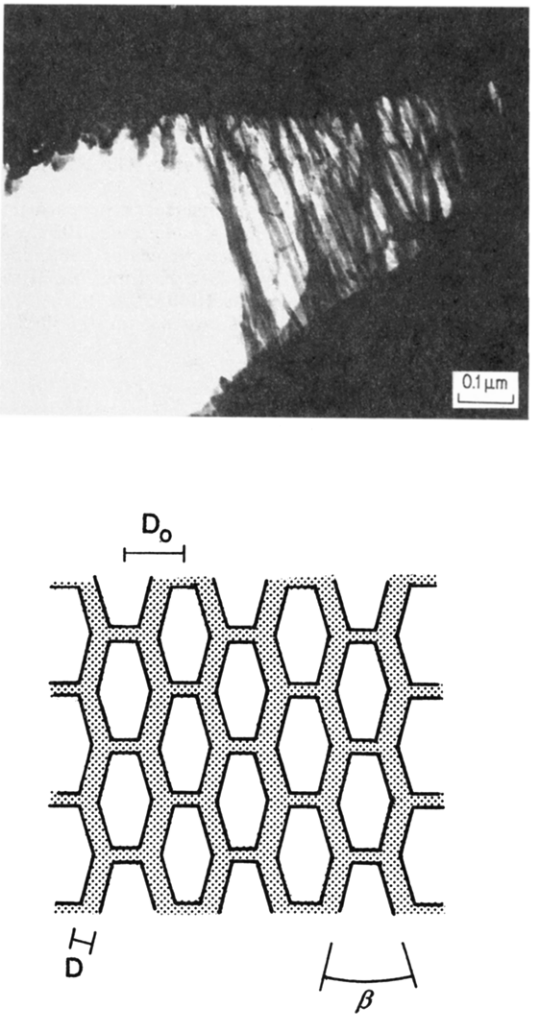

Figure 1. (a, Top) TEM picture of the craze material at a crack tip in polystyrene. (b, Bottom) Schematic microstructure of the craze material, showing both main and cross-tie fibrils.

* To whom correspondence should be addressed.

® Abstract published in *Advance ACS Abstracts,* February 1, 1995.

0024-9297/95/2228-1654$09.00/0

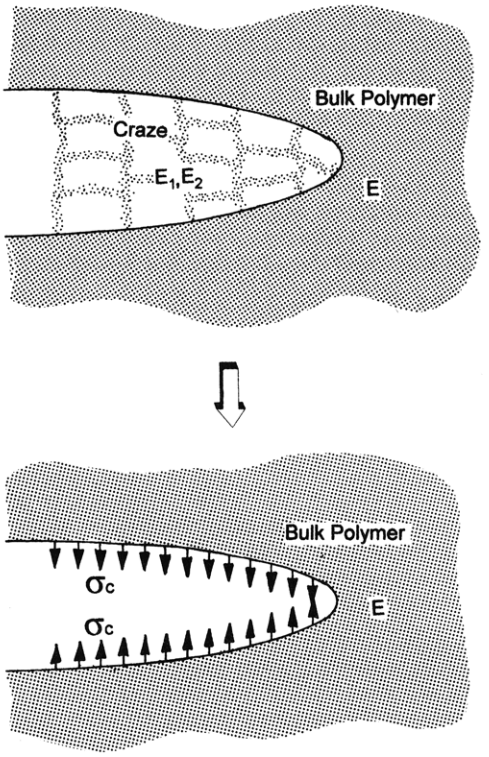

Figure 2. Schematic of the craze zone and the approximate Dugdale model representation. Crazed polymer in the crazing zone is replaced by the crazing stress σ_c applied on the bulk polymer/craze interface.

A widely used model for understanding the craze zone shape is the Dugdale model.[6,7] It is first recognized that the crazing stress σ_c, which is the stress at the craze/bulk interface, is the stress required to draw the fibrils out and so is a material property and is a constant along the whole interface.[1] In the Dugdale model, the crazed material is replaced by the constant stress σ_c along the upper and the lower bulk surfaces representing the closure forces exerted by the bridging fibrils (Figure 2). The size of this Dugdale zone is fixed by the condition that the craze zone bridging eliminates the stress intensity K at the craze tip. The calculated crack face opening displacement in the craze zone gives the approximate craze zone shape and is in good agreement with the experimentally observed shape. However, the Dugdale model does not include the influence of the cross-tie fibrils in the craze, and thus information about the stress distribution in the craze zone near the crack tip is not available; it is assumed to be σ_c. Furthermore, there is no way to predict subsequent craze breakdown at the crack tip without invoking other ad-hoc conditions, such as the existence of a critical crack-opening displacement. Finally, the influence of the craze wake, which appears once the crack does start to grow through the craze, cannot be accounted for in this model.

Brown[8] recently proposed a new model including cross-ties and fibril breakage in the crazing problem, a model subsequently analyzed in more detail by Hui et al.[9] Considering the long slim shape of the craze zone observed experimentally, they used an anisotropic elastic strip embedded in the homogeneous bulk polymer to represent the crazed material. The anisotropy arises from the relative ability of the main aligned fibrils and cross-tie fibrils to carry load. The model successfully predicts a crack tip stress intensity factor K_{tip} as a function of the elastic anisotropy, the craze zone thickness H, the crazing stress σ_c, and the applied stress intensity factor K_{app}. Brown also expressed the critical energy release rate in terms of the single polymer chain breaking force, the areal chain density in the interface, and the elastic moduli ratio in the craze and therefore established a relationship between the micromechanical craze properties and the macromechanical polymer toughness. Two minor limitations of the model are that it cannot provide information about the shape and size of the craze zone nor describe the evolution of the crazing process from craze initiation to crack growth.

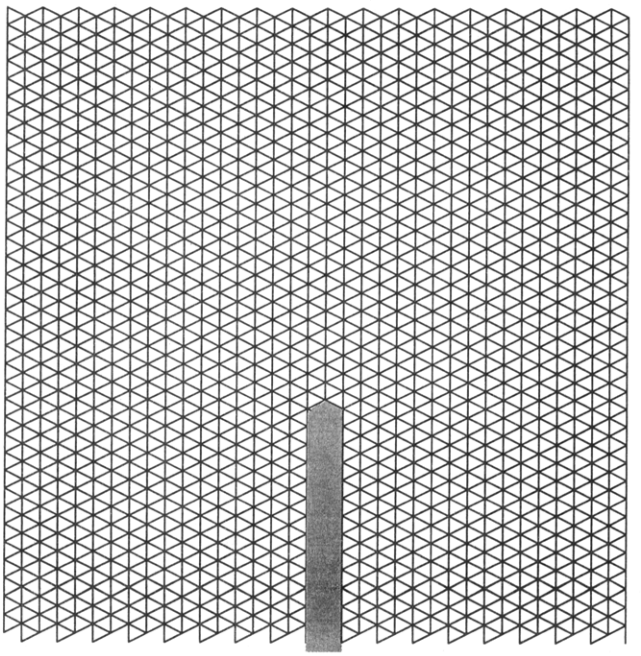

Figure 3. Schematic of the elastic spring network with an embedded crack prior to any deformation. A 75 × 75 node network with size 25 crack is used in the calculations in this work.

II. Elastic Spring Network Model for Craze Growth and Failure

As an alternative approach to the analytic models previously employed, we use a discrete elastic spring network to simulate the behavior of the continuum polymer. Our motivation for this approach is that such a model is simple enough to allow for craze formation and breakdown self-consistently, i.e., in response to the spatially varying stress field established by the presence of the craze itself, with only two simple rules regarding (i) transformation of bulk polymer to craze material and (ii) craze fibril failure under load. As shown in Figure 3, the continuum material is discretized into an equilateral triangular array of nodes connected by linear elastic springs. The triangular node−spring network is used to analyze the stress and strain distribution in the material. The equilibrium lengths r_0 (the unstretched length) of all springs are identical, and the local strain is represented in terms of the spring length r by $\epsilon = (r - r_0)/r_0$. The local stress is related to the force in the spring, and this force in terms of deformation is $F = k^*(r - r_0)/r_0$, where k is the spring constant. The local stress σ and the elastic modulus E are directly related to F and k, respectively, and we will generally use the terms stress and modulus rather than force and spring constant in our subsequent discussions.

This network structure is very convenient to simulate cracks, crack growth, and elastically inhomogeneous material. The values of modulus E and failure stress

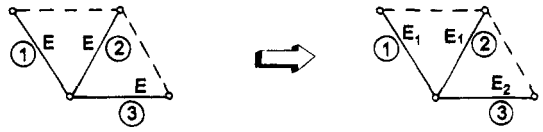

Figure 4. Three-spring unit used in the simulation in the upper half-plane. The parallelogram shows the volume of the material represented by the basic unit. The lower half-plane units are similar.

σ_f can be assigned to each spring individually. By setting the elastic modulus to be 0, one can remove the force-bearing ability of the spring, which is equivalent to embedding a crack in the network. By assigning different elastic moduli to different springs, one can simulate elastically inhomogeneous material; for example, the initial crack at the start of the craze process is generated simply by assigning zero modulus to an array of linear springs, as shown in Figure 3. External loads are applied by fixing the vertical displacement of the bottom line and imposing a uniform displacement along the top line. In general, mechanical equilibrium in the network is achieved by adjusting all of the node positions to balance the forces on each internal node. The force on a spring at the equilibrium state is used to analyze the local stress. Such a technique has been used previously to simulate cracks in a disordered material,[10] various microcrack problems,[11,12] and crack propagation in volume-expanding and microcracked materials.[11]

In applying the spring network to study polymer crazing, we first identify the key physical aspects of the problem which must be retained in the model. First, there exists a "crazing" stress σ_c at which isotropic bulk polymer is drawn out, or transformed, into craze material. Second, the craze material is elastically softer than the bulk polymer, due to the low density of the craze or, equivalently, the high drawing ratio λ of the fibrils. Third, the craze material is elastically anisotropic: the ratio of the moduli E_1 parallel to the drawing direction and E_2 perpendicular to the drawing direction is governed by the cross-tie fibrils (in the absence of the cross-ties, $E_2 = 0$). Fourth, a craze fibril has a maximum tensile strength σ_b which is determined by the strength of a polymer chain, the number of chains in the fibril, and the fibril density per unit area; beyond stress σ_b a fibril breaks and ceases to have any load-bearing capacity.

Since the spring model must incorporate anisotropy in application to the crazing problem and since single springs are just linear tensile springs, we need to define a basic unit or group of springs to which rules will be applied. We select the smallest isotropic unit possible in the triangular lattice, namely, the three-spring unit shown in Figure 4. The springs and the dashed lines in Figure 4 show the volume in the material represented by the three-spring unit. With both this basic unit and the physical aspect of crazing identified above, the rules governing bulk-to-craze transformation and craze failure in our simulation are as follows. Bulk isotropic regions of polymer are represented by the basic parallelogram unit with three equal modulus springs of modulus E. The average of the tensile forces in the near-vertical springs, labeled 1 and 2 in Figure 4, is used as the measure of the tensile stress in the material: $\sigma \propto F = (F_1 + F_2)/2$. Under increasing external load, when $F > F_c$ on any triangular unit, where F_c is the crazing force, the unit is "transformed" to craze material. As shown in Figure 4, a unit of craze material consists of springs 1 and 2 of moduli $E_1 < E$ and a horizontal spring, representing the effect of the cross-tie fibrils, of modulus $E_2 < E_1$. With these two rules, we create soft, anisotropic elastic material simulating the crazed polymer. After the initiation of some crazed material, the network contains two kinds of material, the uncrazed bulk material and the crazed material. *The presence of the craze changes the stress field throughout the material and can induce further craze growth if* $(F_1 \pm F_2) > F_c$ *is satisfied elsewhere in the material.*

Note that our rules for the transformation from bulk to crazelike material *do not* include the large elongation associated with the natural draw ratio λ. Although the spring lengths can in principle be changed to accommodate dilation or extension, it is not appropriate to do so in this case. Practically, a large dilation of the transformed springs is not within the small-strain limit of the spring model and so the induced distortions would be highly nonlinear. Physically, the continuous growth via drawing as modeled using a discrete model probably requires a change in length scale of the discretization after each transformation of a "unit". Our purpose here is mainly to study the *elastic* problem governing craze growth and failure, including the crack tip stress intensity, as considered analytically by Brown and Hui et al. for the fully developed craze. The extension λ contributes to the macroscopic toughness due to the additional work done by the loading system, but it is not expected to greatly modify the other features of craze growth and breakdown. This last point is consistent with the results of Brown and Hui et al. in which the extension λ appears explicitly in the results only as a factor $(1 - 1/\lambda)$ in the overall toughness.

Finally, local craze failure occurs if $(F_1 + F_2)/2 > F_b$ is satisfied in any unit of the craze, where $F_b > F_c$ is the threshold for the craze breakdown. Failure is accomplished by setting the moduli of springs 1 and 2 of that unit to zero.

Figure 4 shows the unit in the upper half-plane. By symmetry and to maintain a well-defined crack plane in the material, the material in the lower half-plane can be represented by a similar but inverted three-spring parallelogram unit.

In general, with the above simple rules and without explicit drawing, the craze problem as formulated is always a fully elastic problem. A state of mechanical equilibrium at some externally applied load exists when all units of bulk polymer have force $F < F_c$ and all units of craze material have force $F < F_b$. At this point, the craze shape and stress distributions in the entire system can be investigated. Application of a higher external load can then lead to additional craze formation and/or failure to establish a new equilibrium configuration. The evolution of the craze structure is carried out self-consistently by this approach because the local stresses on each unit are determined by the applied loading, the initial crack, and the size and the shape of the evolving craze zone itself.

To overcome some limitations of the finite size of the network, we use a shifting method to simulate crack growth while maintaining constant crack size. Specifically, it turns out that craze failure always occurs at the crack tip because of the stress concentration in the anisotropic craze. So, when the tip unit springs are broken, we shift all the material properties one unit toward the crack instead of increasing the crack length one unit and add new bulk polymer material at the opposite edge of the sample. By this ploy, we allow a

craze wake to form behind the crack but avoid the problem of having the crack approach the opposite free edge of the sample. Without actually extending the crack, we can study the effect of a large amount of crack growth and a large region of crazing without appreciable boundary effects. We began with a 50 × 50 node network but found that, after growing the crazing zone to a certain size, boundary effects became important. In order to reduce the boundary effects, we have used a 75 × 75 node network with a crack size of 25 units for the study presented below. The time required to re-equilibrate stresses after transformation of a single craze unit varies with configuration, and the total time for study of craze growth and failure depends on the F_b/F_c ratio. Typically, a single complete simulation with an intermediate size craze requires roughly 5 CPU hours on a small VAX mainframe computer.

III. Results and Discussion

(I) Craze Zone Formation. Here we dedicate our attention to the craze formation process by not allowing craze failure (i.e., set $F_b = \infty$). In polystyrene (PS), the craze extension ratio is about 4, so that the density of the crazed PS is 1/4 that of the bulk PS, and hence we usually assume $E_1 = E/4$ in this work. Since in the lateral direction the load-bearing ability of the material is lower, we set $E_2 = E_1/2$. The values of these material properties will subsequently be changed to investigate their qualitative effect on the craze zone evolution.

We set the value $F_c = 1$ (F_c is thus the unit of force here). Starting from the precracked homogeneous polymer, we increase the external displacement applied to the network and when the force on the crack tip unit attains F_c, the craze initiation begins by transformation of this unit to crazed material, as shown in Figure 5a. Transformation of the tip unit increases the forces in the neighboring units, but not sufficiently to make them exceed F_c. Further increases in the displacement are needed to transform the unit next to the crack tip. Subsequent units in front of the growing craze are transformed one by one with the increasing loading, leading to the configuration in Figure 5b. With further increasing load the next units transformed are the units on the *second row* near the crack tip, i.e., the craze begins to thicken. After thickening, the craze zone extends one unit forward along the original crack line *without a further increase in external load*, the extension being driven by the stress redistribution, as shown in Figure 5c. The sequence of craze formation driven by increased applied load followed by craze formation driven by the local stress increase caused by stress redistribution due to the craze growth itself continues in this manner, as shown in (d)−(g) of Figure 5. In Figure 5h, the craze propagates all the way to the other edge of the network, forming a slim craze band through the material. In general, the length and the thickness of the craze zone increase alternately as loading continues. Various craze zone shapes obtained under increasing applied displacement beyond that shown in Figure 5 are shown in Figure 6a−d, where it is evident that the shape of the craze zone is continually similar to the one predicted by the Dugdale model. Also, by construction, the stresses in the bulk polymer adjacent to the craze zone are less than σ_c. Along the outer boundary of the craze, and far from the crack tip, the stress in the craze material is also nearly constant, as in the Dugdale model. The network model thus qualitatively produces the results of the Dugdale continuum

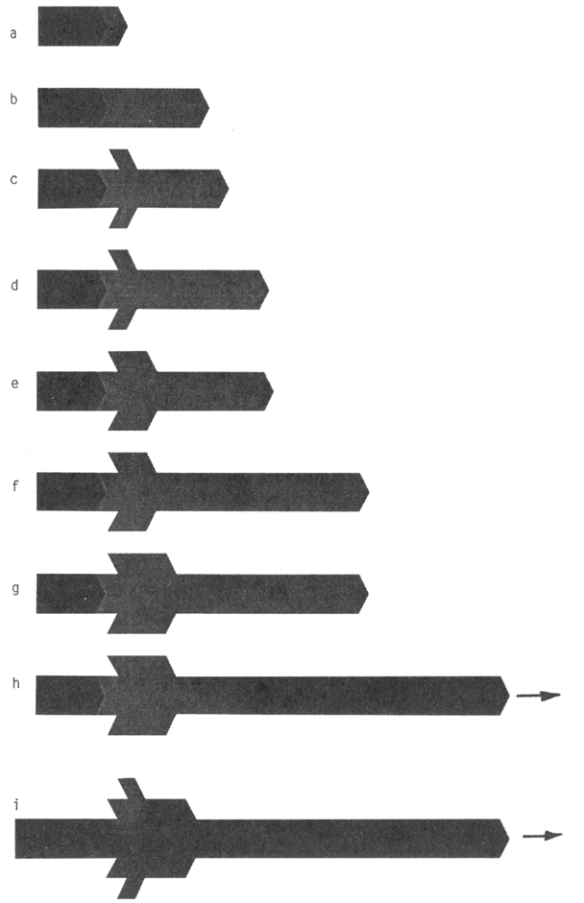

Figure 5. Craze zone formation process with increasing external applied displacement without fibril breaking ($F_b = \infty$). (a) The first unit is transformed into a craze. The crack tip stress/crazing stress ratio is $\sigma_{tip}/\sigma_c = 1$. (b) Four additional units in the crack plane have crazed, and $\sigma_{tip}/\sigma_c = 1.18$. (c) One unit on the second row crazes, and the stress redistribution after the transformation causes craze elongation along the crack plane, $\sigma_{tip}/\sigma_c = 1.05$. (d) The craze zone further elongates with the increasing external load, and $\sigma_{tip}/\sigma_c = 1.27$. (e) The craze extends further just above the crack plane, and $\sigma_{tip}/\sigma_c = 1.32$. (f) The craze further elongates along the crack plane, and $\sigma_{tip}/\sigma_c = 1.47$. (g) The craze extends further just above the crack plane, and $\sigma_{tip}/\sigma_c = 1.53$. (h) The craze along the crack plane propagates across the material to the other edge of the network (not shown). The craze extends further above the crack plane, and $\sigma_{tip}/\sigma_c = 1.64$. (i) The craze elongates on the row above the crack plane and thickness into the third row, and $\sigma_{tip}/\sigma_c = 1.68$.

model. However, in distinct contrast to the Dugdale model, there is a stress concentration in the craze near the original crack tip which ultimately causes the craze failure, as demonstrated in the following section.

(2) Fracture and Craze Zone Propagation. By setting the craze fibril breaking force F_b to a *finite* value, craze breakdown interrupts the zone formation because the stress concentration at the crack tip allows that craze unit to attain a force F_b even though the majority of the craze zone carries a stress close to $F_c < F_b$. Once the crack grows, however, *a wake of previously crazed material exists above and below the crack faces and this wake helps shield the crack tip craze from the applied stress*. To continue driving the crack thus requires increased loading to overcome the additional shielding of the craze wake. Such increased resistance to crack growth from wake formation is well known in ceramic materials such as transformation-toughened zirconia. Increased loading can then also lead to lengthening and/or thickening of the frontal craze zone and hence again

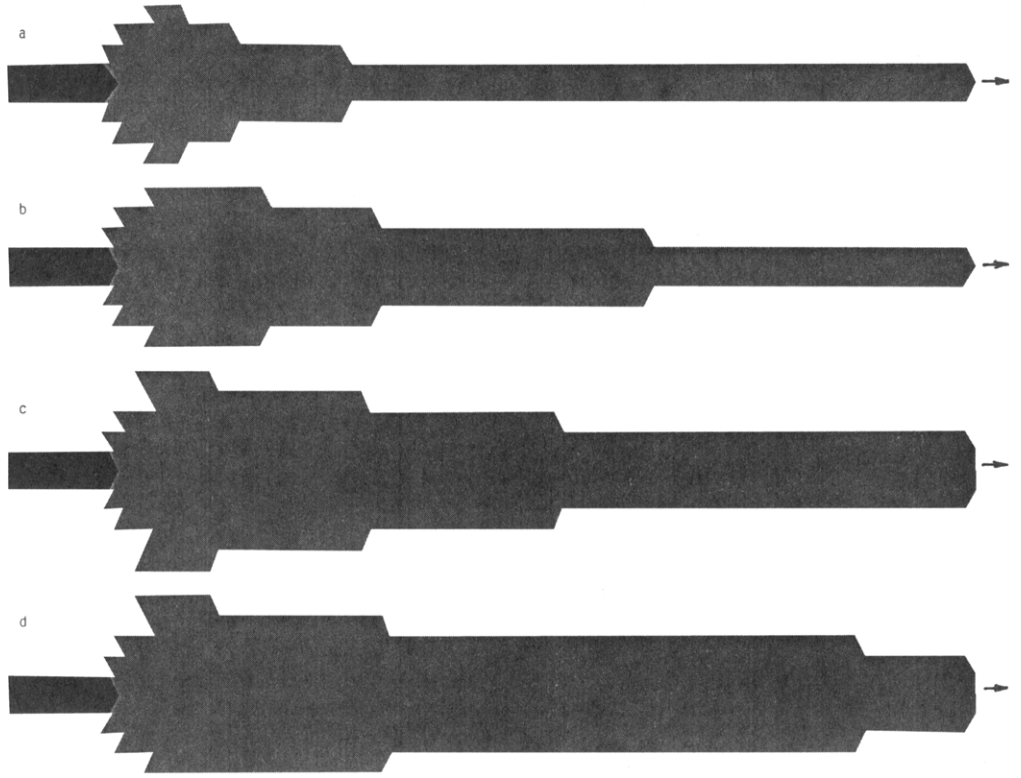

Figure 6. Craze zone configuration at different external load levels: (a) $\sigma_{tip}/\sigma_c = 1.73$; (b) $\sigma_{tip}/\sigma_c = 1.8$; (c) $\sigma_{tip}/\sigma_c = 1.87$; (d) $\sigma_{tip}/\sigma_c = 2.26$.

modify the stress intensity at the crack tip. This entire craze failure process involving failure, growth, and feedback can be investigated by the present simulation model. As an example, the breaking process for the case in which $F_b = 1.47F_c$ is shown in Figure 7. Early in the craze evolution, before the stress at the crack tip reaches the breaking threshold F_b, the transformation is identical to that shown in Figure 5a–f. The initial configuration just before the first breakage is also shown in Figure 7a. With a further increase in the applied displacement, the stress in the crack tip unit exceeds the breaking stress $F_b = 1.47F_c$ for the first time. The bonds in the crack tip units are then broken and all the elements shifted left to simulate the crack extension and wake formation without an increase in the crack length. The craze zone just after the shifting is shown in Figure 7b. The additional shielding from the wake causes $F_{tip} < F_b$ and thus allows increased applied stress and further growth of the craze before the crack tip units again attain stress F_b. Before the second breakage at the crack tip, the craze zone evolves to the configuration shown in Figure 7c. The material along the crack line is crazed to the edge of the network and the craze has thickened to include two units on the third row. A further stress or displacement increase then causes the stress at the tip units to exceed F_b and the units to be broken. Continuing the process of increasing the displacement leads to alternating stable crazing and cracking. The crack zone configurations before the third and fourth tip unit broken are given in (d) and (c) of Figure 7. Ultimately, the craze wake becomes long enough that a stable crazing zone is formed: the craze zone formation and failure produce the same craze configuration with no increase in shielding of the crack tip, and hence no increase in applied displacement is required to continue driving the crack. The final "steady-state" zone for $F_b = 1.47F_c$ is shown in Figure 8b.

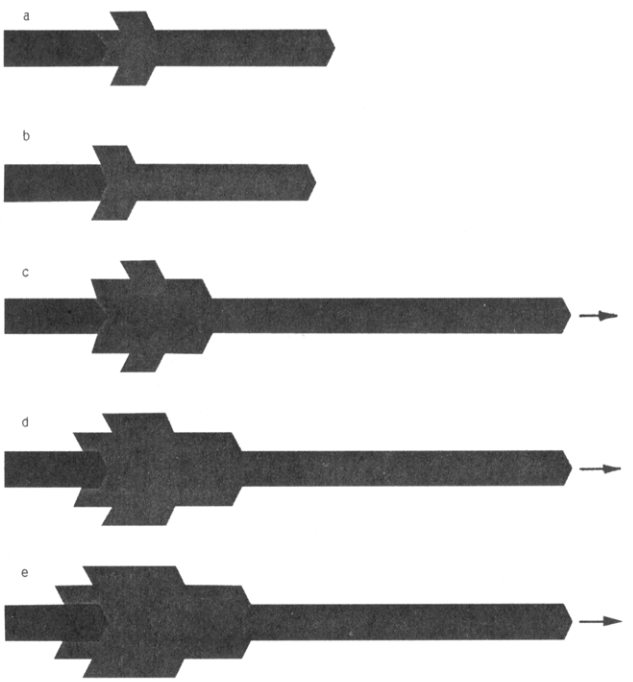

Figure 7. Evolution of the craze formation and breakdown for $F_b/F_c = 1.47$: (a) craze zone shape before the first breakage (as in Figure 5f); (b) craze zone shape just after the first breakage and shifting; (c) craze zone configuration before the second breakage at the crack tip (the craze has propagated to the other edge of the network); (d) craze zone configuration before the third breakage at the crack tip. (e) craze zone configuration before the fourth breakage at the crack tip.

Increasing the F_b/F_c ratio allows the initial craze zone to develop further prior to crack propagation as shown in Figure 6a–d, but the general sequence of crazing and craze breakdown for each case is similar to that described above for the $F_b = 1.47F_c$ case. We present the final stabilized craze zones for $F_b/F_c = 1.2$, 1.47, 1.6,

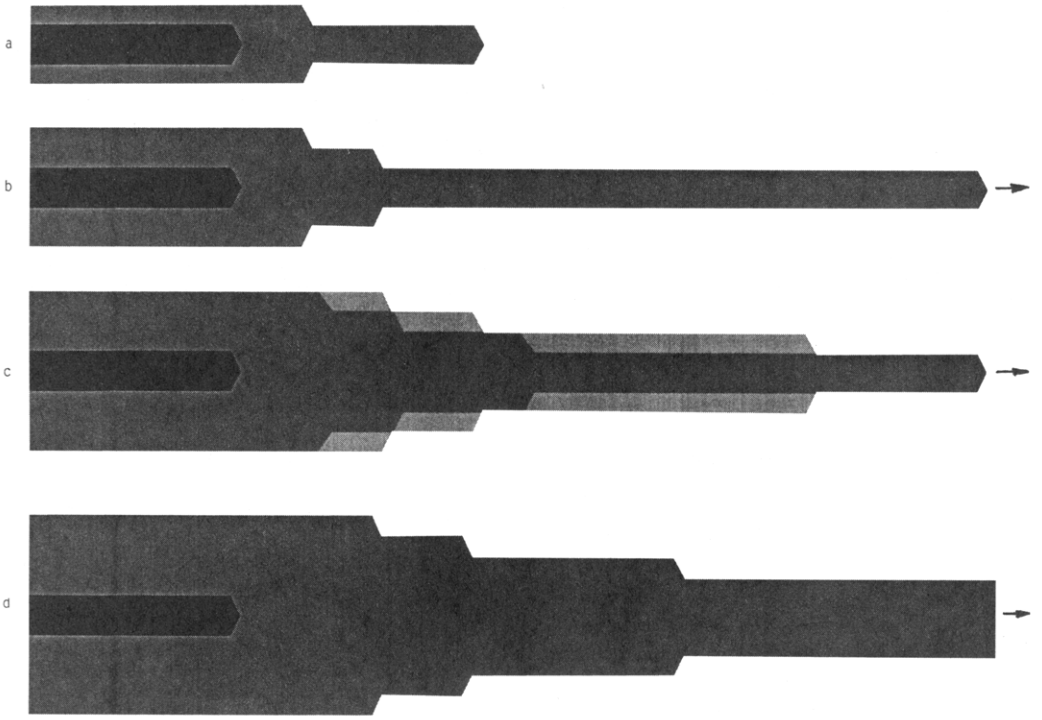

Figure 8. Stable craze zone profiles at different F_b/F_c ratios: (a) $F_b/F_c = 1.2$; (b) $F_b/F_c = 1.47$; (c) $F_b/F_c = 1.6$ and 1.73 (additional light gray regions); (d) $F_b/F_c = 1.8$.

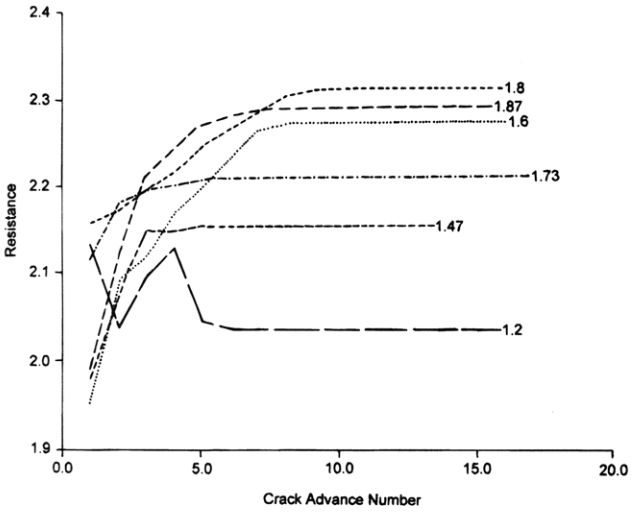

Figure 9. Resistance curve K_R vs Δc (crack tip shielding vs crack growth) for various F_b/F_c. The resistance factor is $K_R = \sigma^0_{tip}/\sigma^c_{tip}$, where σ^0_{tip} and σ^c_{tip} are the stresses at the tip without and with the craze at the same external *load* level, respectively.

1.73, and 1.8 in Figure 8a–d. As F_b/F_c increases, the craze zone is elongated and thickened, and larger craze zones lead to increased shielding at the crack tip, and hence increased macroscopic toughness. We use the ratio of the stress at the crack tip without and with the craze (σ^0_{tip} and σ^c_{tip}, respectively) as a measure of the shielding effect or increased toughness due to craze. Using language similar to that in the ceramics field, we will call the ratio $K_R = \sigma^0_{tip}/\sigma^c_{tip}$ the resistance factor. The resistance factor as a function of the crack advance length is given in Figure 9. The curves are quite smooth after the crack has advanced a few units and indicate the increasing crack tip shielding caused by the craze wake.

Figure 9 demonstrates some distinct effects of our use of a discrete lattice model. For instance, the resistance curve for the $F_b/F_c = 1.2$ case is not smooth at the beginning. The peak in the curve (a high shielding effect) is caused by a temporary craze widening into the third row, which then moved into the crack wake, with no further craze formed in the third row. As the unusual craze unit moves further into the wake, the shielding decreases and becomes smooth. Another phenomenon due to the discrete lattice is that the shielding effect of the $F_b/F_c = 1.73$ case is lower than that of the $F_b/F_c = 1.6$ case. But if we look at the final profile of the craze zones in Figure 8, we find that in the $F_b/F_c = 1.73$ case the craze zone is stretched longer but not thicker than the one in the $F_b/F_c = 1.6$ case. The long narrow craze zone has a higher stress concentration at the crack tip, since the load-bearing ability of the crazed tail is lower. As noted, such nonmonotonic behavior is largely attributed to the discrete lattice. For the craze to thicken by one unit requires a finite stress increase—the discrete lattice does not allow a continuous thickening—while lengthening along the craze can occur with lower stress increases and in a more continuous manner. Thus, some behavior when considered in detail is an artifact of the fairly coarse scale (spring length versus crack length) of the present network simulations. Nonetheless, the overall behavior of craze growth is well captured by the discrete model.

We have also investigated the thickness of the steady-state crazing zone H and its relation with the stress intensity at the crack. The stress intensity factor K_{tip} *is measured by the stress at the crack tip, which is close to the assigned craze fibril breaking threshold* F_b, and the craze thickness is given by the number of rows in the craze zone near the crack tip. The stress intensity factor K_{tip} is normalized by the crazing stress σ_c to $K^*_{tip} = K_{tip}/\sigma_c$. The K^*_{tip}–H relation is plotted in Figure 10. From curve fitting of the data points, the relation is very nearly $K^*_{tip} \sim H^{1/2}$; i.e., the stress intensity at the crack tip in the craze zone is proportional to the square root of the craze zone thickness and proportional to the crazing stress σ_c. This result agrees precisely with the

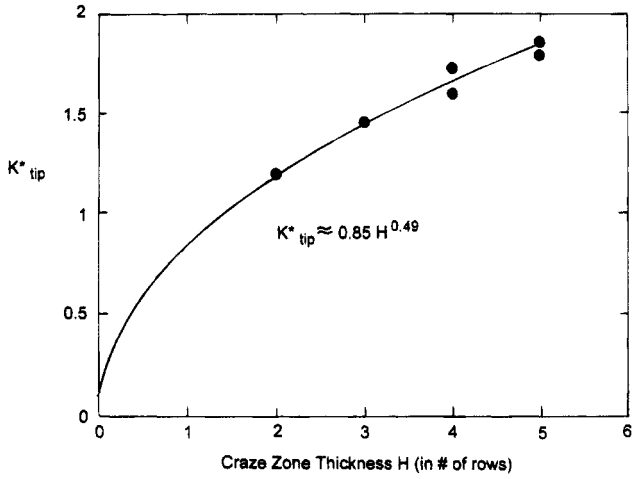

Figure 10. Steady-state stress concentration at the crack tip, $K^*_{tip} = K_{tip}/\sigma_c$, vs craze zone thickness H at the crack tip, and a power law fit demonstrating $K^*_{tip} \propto H^{1/2}$, as predicted in analytical models.[9,10]

results given by Brown[8] and Hui[9] obtained from an anisotropic continuum mechanics analysis.

We have also qualitatively investigated the effect of the ratios E_1/E and E_2/E_1 on the entire process. As seen in Figure 4, if E_1/E is lowered, the crazed material is more compliant in the vertical direction, the load-bearing capability of the crazed material is lower, and so the craze zone will grow longer at lower applied loads; such behavior is observed in the simulation. If the E_2/E_1 is lowered, the horizontal spring in a craze unit (#3 in Figure 4) provides less resistance and the unit becomes more compliant in the vertical direction so that the effect of lower E_2/E_1 also produces a longer craze zone. A lower E_2/E_1 ratio also leads to slightly lower stress concentration at the crack tip, which qualitatively agrees with the result of Brown and Hui et al. Notice that the moduli E_1 and E_2 in this work are related to the E_1 and E_2 in ref 8 and C_{22} and C_{12} in ref 9, but they are *not* exactly the same, so one should not compare the quantitative effects of moduli variations in the network model directly to the corresponding results in refs 8 and 9.

IV. Conclusions

A spring network has been used to simulate craze formation, growth, and breakdown in a generic glassy polymer. With a few simple rules, the model reproduces the qualitative features observed in experiments. The stress in the network generated by the remote loading induces the formation of the craze. The low modulus of the craze material and its elastic anisotropy drive the craze zone ahead of the crack and also produce a stress concentration at the crack tip which ultimately causes the craze breakdown. The entire crazing process is simulated self-consistently: starting from a bulk polymer with an initial crack and with the values F_c and F_b for the craze formation and craze breakdown thresholds fixed at the outset, the simulation generates the stress distributions and craze zone development with no further input. The simulation model produces craze zone profiles similar to those observed experimentally and provides useful qualitative information about the stress distribution in the crazed and bulk materials. By varying the F_b/F_c ratio, we have further demonstrated how the extent of stable crack growth and macroscopic toughness of the material are controlled by the underlying craze stress $\sigma_c \sim F_c$, craze elasticity moduli (E_1 and E_2), and craze fibril breakdown strength $\sigma_b \sim F_b$. Although the present results serve mainly to support some recent theoretical developments,[8,9] the numerical technique used here may find applications in craze problems involving material heterogeneity or other types of defects, problems which may not be analytically tractable at present.

Acknowledgment. We gratefully acknowledge useful discussions with Professor E. J. Kramer at the outset of this work and with Professor C. Y. Hui. F.X. acknowledges summer support by BP Research.

References and Notes

(1) For a recent review, see: Kramer, E. J.; Berger, L. L. *Adv. Polym. Sci.* **1990**, *91/92*, 1.
(2) Kramer, E. J. *Adv. Polym. Sci.* **1983**, *53*, 1.
(3) Lautwasser, B. D.; Kramer, E. J. *Philos. Mag.* **1979**, *A39*, 469. Brown, H. *J. Mater. Sci.* **1979**, *14*, 237.
(4) Donald, A. M.; Kramer, E. J. *J. Polym. Sci., Polym. PHys. Ed.* **1982**, *20*, 899.
(5) Miller, P.; Buckley, D. J.; Kramer, E. J. *J. Mater. Sci.* **1991**, *26*, 2815.
(6) Dugdale, D. S. *J. Mech. Phys. Solids* **1960**, *8*, 100.
(7) Brown, H.; Ward, I. M. *Polymer* **1973**, *14*, 469.
(8) Brown, H. R. *Macromolecules* **1991**, *24*, 2752.
(9) Hui, C. Y.; Ruina, A.; Creton, C.; Kramer, E. J. *Macromolecules* **1992**, *25*, 3948.
(10) Curtin, W. A.; Scher, H. *J. Mater. Res.* **1990**, *5*, (3), 535. Sahimi, M.; Goddard, J. D. *Phys. Rev. Lett.* **1986**, *33*, 7848. Termonia, Y.; Meakin, P. Nature **1986**, *320*, 429. Duxbury, P. M.; Leath, P. L.; Beale, P. D. *Phys. Rev. B* **1987**, *36*, 367. Beale, P. D.; Srolovitz, D. J. *Phys. Rev. B* **1988**, *37*, 5500. Khang, B.; Batrouni, G. G.; Redner, S.; deArcangelis, L.; Herrmann, H. J. *Phys. Rev. B* **1988**, *37*, 7625. Herrmann, H. J.; Hansen, A.; Roux, S. *Phys. Rev. B* **1989**, *39*, 637. deArcangelis, L.; Herrmann, H. J. *Phys. Rev. B* **1989**, *39*, 2678.
(11) Curtin, W. A.; Scher, H. *J. Mater. Res.* **1990**, *5* (3), 554.
(12) Curtin, W. A.; Futamura, K. *Acta Metall. Mater.* **1990**, *538* (11), 2051.

MA941271V